DOI: 10.1002/ange.200701694

Reactions of FeO Nanoparticles

Controlled Synthesis and Chemical Conversions of FeO Nanoparticles**

*Yanglong Hou, Zhichuan Xu, and Shouheng Sun**

Transition metal oxide nanoparticles of type MO, where M is Mn, Co, Ni, or Fe, have attracted tremendous interest recently because of their potential as electrode materials for rechargeable solid-state batteries,[1] as efficient catalysts for fuel-cell reactions,[2] and as nanoscale magnetic models for understanding nanomagnetism.[3] Wüstite (FeO) is one form of the common iron oxides, a group that also includes hematite (α-Fe_2O_3), maghemite (γ-Fe_2O_3), and magnetite (Fe_3O_4). It has a rock-salt structure with Fe and O forming nonstoichiometric Fe_xO ($x = 0.83$–0.96) and Fe vacancies in an ordered distribution.[4] The structure is not chemically stable and is prone to decomposition into α-Fe and inverse spinel Fe_3O_4 through a two-step disproportionation process or to oxidation to form Fe_3O_4, γ-Fe_2O_3, and/or α-Fe_2O_3.[4] This chemical reactivity makes FeO nanoparticles difficult to make and those prepared from the high-temperature solution-phase decomposition of iron salt have not been fully characterized.[5]

Herein we report a facile organic-phase synthesis of monodisperse FeO nanoparticles through high-temperature reductive decomposition of iron(III) acetylacetonate ([Fe(acac)$_3$]) with oleic acid (OA) and oleylamine (OAm) both as surfactants and solvents. The sizes of the particles are tuned from 14 to 100 nm by controlling the heating conditions and the shapes of the particles are controlled to be either spherical or truncated octahedral depending on the volume ratio of OA and OAm used in the reaction. Thermal annealing under an argon atmosphere converted these FeO nanoparticles into composite Fe–Fe_3O_4 nanoparticles, while controlled oxidation of the FeO nanoparticles resulted in the formation of Fe_3O_4, γ-Fe_2O_3, or α-Fe_2O_3 nanoparticles. These monodisperse FeO nanoparticles have great potential for catalysis[2c–f] and gas-sensor[2g] applications. The chemical conversions of the paramagnetic FeO nanoparticles may also be considered as an alternative, yet better, approach to the synthesis of various magnetic iron oxide or iron nanoparticles with sizes that are difficult to achieve from previous organic-phase syntheses.[6]

The nanoparticles were grown from the reaction mixture ([Fe(acac)$_3$] in a mixture of OA and OAm) by controlled heating at 220 °C and 300 °C. In the presence of an excess amount of OAm, spherical nanoparticles were formed, whereas in the presence of equivalent amounts of OA and OAm, truncated octahedral nanoparticles were obtained. The size of both kinds of nanoparticles was tuned by simply controlling the period of heating at 220 °C and 300 °C. For example, 14-nm spherical nanoparticles were synthesized by treating [Fe(acac)$_3$] with OA (8 mL) and OAm (12 mL) at 220 °C and 300 °C, each for 30 min. Extended heating at 300 °C for 1 h gave 22-nm nanoparticles. Heating of a reaction mixture of [Fe(acac)$_3$], OA (10 mL), and OAm (10 mL) at 220 °C and 300 °C, each for 30 min, led to the formation of 32-nm truncated octahedral nanoparticles, while heating of the mixture at 220 °C for 1 h and at 300 °C for 30 min gave 53-nm nanoparticles and heating at 220 °C for 30 min and at 300 °C for 1 h yielded 100-nm truncated octahedral nanoparticles.

Figure 1 shows transmission electron microscopy (TEM) images of representative FeO nanoparticles. The truncated octahedral shape of the particles can be better seen in the scanning electron microscopy (SEM) image of Figure 1 d.

These size- and shape-controlled syntheses suggest that 1) the use of OA and OAm both as solvents and surfactants facilitates the formation and stabilization of FeO nanoparticles; 2) the presence of an excess of OAm facilitates

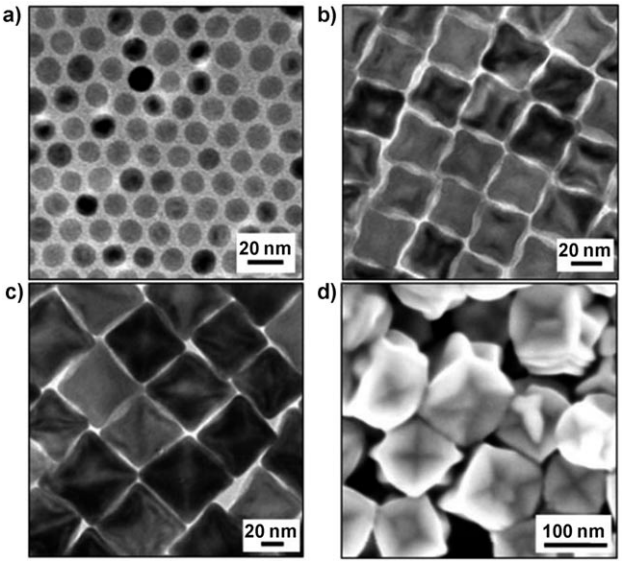

Figure 1. TEM images of FeO nanoparticles (the sizes refer to the average lengths of one side in the projected images): a) 14-nm spherical, b) 32-nm, and c) 53-nm truncated octahedral. d) SEM image of 100-nm truncated octahedral nanoparticles.

[*] Dr. Y. Hou, Z. Xu, Prof. S. Sun
Department of Chemistry
Brown University
Providence, RI 02912 (USA)
Fax: (+1) 401-863-9046
E-mail: ssun@brown.edu

[**] This work was supported by ONR/MURI under grant no. N00014-05-1-0497, NSF/DMR under grant no. 0606264, and INSIC. We thank Dr. Y. Ding at the Georgia Institute of Technology for his help with the high-resolution transmission-electron-microscopy analysis of the FeO nanoparticles.

Supporting information for this article is available on the WWW under http://www.angewandte.org or from the author.

growth in all crystal planes on the surface of the FeO nuclei, thereby giving spherical nanoparticles—this may be explained by the fact that extra OAm acts as a weaker ligand during the reaction and there is negligible energy difference for OAm to dissociate from different crystal planes on the surface of the nuclei during the high-temperature growth process; and 3) the 1:1 volume ratio of OA:OAm presents enough OA to regulate the competitive growth in the ⟨100⟩ direction over the ⟨111⟩ direction, a process leading to the formation of the truncated octahedron. Although the detailed growth mechanism is not completely understood, it is worth noting that the shape-controlled synthesis reported herein bears some similarity to the synthesis of rare-earth metal oxide nanoparticles in the presence of oleic acid and oleylamine. The binding difference between oleate and oleylamine on the crystal planes decides the final shape of the nanoparticles.[7]

An X-ray diffraction (XRD) study shows that the as-synthesized FeO nanoparticles have a face-centered cubic (fcc) structure and the peak width of the diffraction pattern is size dependent. Figure 2 shows the XRD patterns of the 14-, 32-, 53-, and 100-nm FeO nanoparticles, with the (111), (200), (220), (311), and (222) peaks from the fcc structure clearly identified. The shoulder at 34.5°, which becomes more apparent in the patterns from the smaller nanoparticles, is due to surface oxidation of the FeO nanoparticles and the formation of a layer of Fe_3O_4 coating. The average (200) correlation size was estimated with Scherrer's formula to be 13.5 nm in Figure 2a, 31 nm in Figure 2b, 52 nm in Figure 2c, and 98 nm in Figure 2d. These sizes are consistent with those measured from the TEM images, a result indicating that the nanoparticles have a single crystal structure. The structure of a single nanoparticle was studied by high-resolution TEM (HRTEM), as shown in Figure S1 in the Supporting Information. The nanoparticle has a core/shell FeO/Fe_3O_4 structure with both the core and shell being well crystallized.

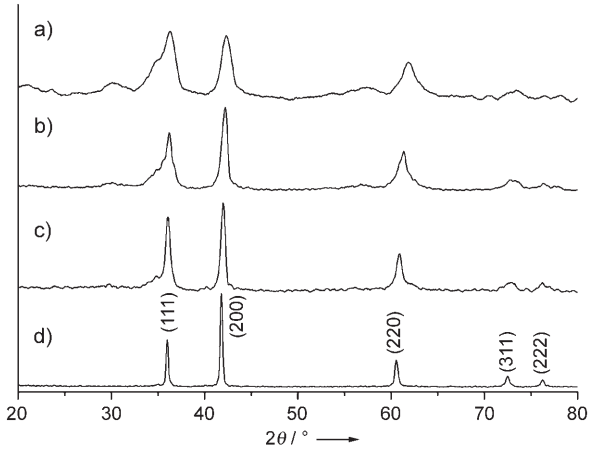

Figure 2. XRD patterns of as-synthesized FeO nanoparticles with sizes of a) 14, b) 32, c) 53, and d) 100 nm.

The as-synthesized FeO nanoparticles do not undergo fast oxidation under ambient conditions. An XRD study on the 53-nm nanoparticle assembly shows no apparent deep oxidation after purification and separation in air during the synthesis. This is different from the previous observations that FeO nanoparticles are not stable and are prone to oxidation.[5] At elevated temperatures, however, the as-synthesized FeO nanoparticles undergo chemical and structural conversions into various iron oxide nanoparticles. Figure 3 shows the XRD patterns of the 32-nm FeO nanoparticles and the iron oxide nanoparticles obtained from their controlled oxidation. When annealed under atmospheric pressure and air, the FeO nanoparticles (Figure 3a) are converted into Fe_3O_4 nanoparticles (at 120 °C for 90 min, Figure 3b), γ-Fe_2O_3 nanoparticles (at 200 °C for 30 min, Figure 3c), or α-Fe_2O_3 nanoparticles (at 500 °C for 120 min, Figure 3d). The γ-Fe_2O_3 nanoparticles are characterized by a peak shift to higher angles and the appearance of two characteristic superlattice diffractions from the (210) and (213) planes at lower angles (around 24° and 26°, respectively). These nanoparticles are also characterized by their conversion into α-Fe_2O_3 at 500 °C under Ar.[4,5b] TEM image analysis indicates that the annealed nanoparticles show negligible morphology change during the oxidative annealing processes.

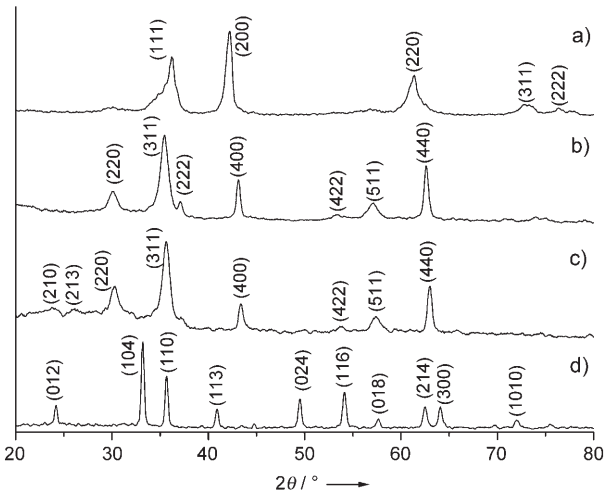

Figure 3. XRD patterns of iron oxide nanoparticles: a) FeO, b) Fe_3O_4, c) γ-Fe_2O_3, and d) α-Fe_2O_3.

The FeO nanoparticles are also subject to disproportionation under controlled annealing conditions. For example, the 53-nm FeO nanoparticles can be converted into composite nanoparticles of Fe and Fe_3O_4 after annealing at 500 °C under an argon atmosphere for 1 h followed by 1 K min^{-1} cooling. The XRD pattern of the composite nanoparticles shows clearly the body-centered cubic (bcc) Fe and Fe_3O_4 peaks (Figure S2 in the Supporting Information). Figure S3 in the Supporting Information shows the TEM image of the 53-nm FeO nanoparticles after the disproportionation reaction, with smaller dark dots indicating Fe and lighter large particles indicating Fe_3O_4. The interfringe spacing is 0.21 nm within the smaller dot (Figure S3c in the Supporting Information) and 0.29 nm in the larger particle (Figure S3d in the Supporting Information). The 0.21-nm spacing is close to 0.203 nm, the

interplane distance of the (110) planes of bcc Fe, while the spacing of 0.29 nm matches with the interplane distance of 0.296 nm for the (220) planes in Fe_3O_4.

The formation of various iron oxide and iron nanoparticles from controlled chemical conversions of the FeO nanoparticles indicates that the magnetic properties of the nanoparticles prepared from these FeO nanoparticles can be readily tuned. Figure 4 shows a series of hysteresis loops for

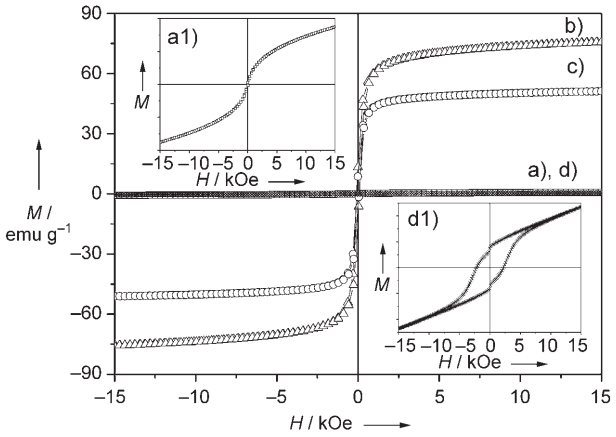

Figure 4. Room-temperature hysteresis loops of a) as-synthesized 32-nm truncated octahedral FeO nanoparticles (inset a1: a close look at a section of trace (a)), b) Fe_3O_4 nanoparticles, c) γ-Fe_2O_3 nanoparticles, and d) α-Fe_2O_3 nanoparticles (inset d1: a close look at a section of trace (d)).

iron oxide nanoparticles made from the FeO nanoparticles. The as-synthesized 32-nm FeO nanoparticles are almost paramagnetic (Figure 4a and the corresponding inset); the Fe_3O_4 coating results in a slight deviation from paramagnetic behavior. Both Fe_3O_4 (Figure 4b) and γ-Fe_2O_3 (Figure 4c) nanoparticles exhibit superparamagnetic behavior, with the magnetic moments reaching 75 (Fe_3O_4) and 51 emu g^{-1} (γ-Fe_2O_3), respectively. In contrast to Fe_3O_4 and γ-Fe_2O_3, the α-Fe_2O_3 nanoparticles show a much lower magnetic moment at less than 1 emu g^{-1}, which is close to that from the bulk hematite (0.4 emu g^{-1}), and a hysteresis behavior at room temperature,[4] which indicates a dramatic structural change within the particles. As a comparison, the magnetic moment of the composite α-Fe and Fe_3O_4 nanoparticles reaches 120 emu g^{-1}.

We have reported a simple process for preparing monodisperse FeO nanoparticles through a high-temperature reaction of [$Fe(acac)_3$] with oleic acid and oleylamine. The sizes of the nanoparticles are tunable from 14 to 100 nm and the shapes can be controlled to be either spherical or truncated octahedral. Under controlled annealing conditions, the as-synthesized FeO nanoparticles are converted into Fe_3O_4, γ-Fe_2O_3, or α-Fe_2O_3 nanoparticles or they undergo disproportionation to form Fe–Fe_3O_4 composite nanoparticles. These chemical conversions of the paramagnetic FeO nanoparticles facilitate the one-step production of various iron-based nanomaterials with controlled sizes and tunable magnetic properties for various nanoscale magnetic and catalytic applications.

Experimental Section

Synthesis of 14-nm spherical FeO nanoparticles: [$Fe(acac)_3$] (1.4 g, 4 mmol), OA (8 mL, 25 mmol), and OAm (12 mL, 35 mmol) were mixed and stirred in a three-necked flask. The mixture was heated at 120 °C with vigorous stirring for 2 h. During this time, a partial vacuum was applied to the system to remove trace moisture and oxygen trapped in the reaction system, thereby giving a clear dark-brown solution. Under an Ar blanket, the solution was heated to 220 °C and kept at this temperature for 30 min before it was heated to 300 °C at a heating rate of 2 K min^{-1} and kept at 300 °C for 30 min. The solution was cooled down to room temperature by removing the heating mantle and the FeO nanoparticles were separated upon addition of ethanol (20 mL); this was followed by centrifugation. The nanoparticles were redispersed into hexane and precipitated out by addition of ethanol to further purify them. The final product was dispersed in hexane and stored under a nitrogen atmosphere.

Under similar reaction conditions, spherical FeO nanoparticles with sizes up to 22 nm could be produced by simply extending the heating time at 300 °C.

Synthesis of 32-nm truncated octahedral FeO nanoparticles: [$Fe(acac)_3$] (1.4 g), OA (10 mL), and OAm (10 mL) were mixed and stirred in a three-necked flask. The mixture was heated to 120 °C with vigorous stirring and kept at that temperature for 2 h. During this time, a partial vacuum was applied to the system to remove trace moisture and oxygen trapped in the reaction system, thereby giving a clear dark-brown solution. The solution was heated at 220 °C for 30 min before it was heated to 300 °C at a heating rate of 2 K min^{-1} and kept at 300 °C for 30 min. The workup procedures were the same as those in the synthesis of the 14-nm spherical FeO nanoparticles. The nanoparticles were dispersed in hexane and stored under a nitrogen atmosphere.

Under similar reaction conditions, the sizes of the octahedral FeO nanoparticles were tuned from 32 to 100 nm by controlling the heating time. For example, the mixture was heated at 220 °C for 1 h and at 300 °C for 30 min to prepare 53-nm nanoparticles, while heating at 220 °C for 1 h and at 300 °C for 1 h led to 100-nm nanoparticles.

Received: April 17, 2007
Published online: July 23, 2007

Keywords: disproportionation · iron · nanoparticles · oxidation · oxides

[1] a) P. Poizot, S. Laruelle, S. Grugeon, L. Dupont, J.-M. Tarascon, *Nature* **2000**, *407*, 496–499; b) N. R. Jana, Y. F. Chen, X. G. Peng, *Chem. Mater.* **2004**, *16*, 3931–3935; c) J. Park, E. A. Kang, C. J. Bae, J. G. Park, H. J. Noh, J. Y. Kim, J. H. Park, T. Hyeon, *J. Phys. Chem. B* **2004**, *108*, 13594–13598; d) W. S. Seo, J. H. Shim, S. J. Oh, E. K. Lee, N. H. Hur, J. T. Park, *J. Am. Chem. Soc.* **2005**, *127*, 6188–6189; e) D. Zitoun, N. Pinn, N. Frolet, C. Belin, *J. Am. Chem. Soc.* **2005**, *127*, 15034–15035; f) K. An, N. Lee, J. Park, S. C. Kim, Y. Hwang, J. G. Park, J. Y. Kim, J. H. Park, M. J. Han, J. J. Yu, T. Hyeon, *J. Am. Chem. Soc.* **2006**, *128*, 9753–9760; g) J. S. Do, C. H. Weng, *J. Power Sources* **2006**, *159*, 323–327; h) A. Lagunas, A. M. I. Payeras, C. Jimeno, M. A. Pericas, *Chem. Commun.* **2006**, 1307–1309; i) S. A. Needham, G. X. Wang, H. K. Liu, *J. Power Sources* **2006**, *159*, 254–257; j) T. Ould-Ely, D. Prieto-Centurion, A. Kumar, W. Guo, W. V. Knowles, S. Asokan, M. S. Wong, I. Rusakova, A. Luttge, K. H. Whitmire, *Chem.*

Mater. **2006**, *18*, 1821 – 1829; k) X. Zhong, R. Xie, L. Sun, I. Lieberwirth, W. Knoll, *J. Phys. Chem. B* **2006**, *110*, 2 – 4.

[2] a) J. B. Reitz, E. I. Solomon, *J. Am. Chem. Soc.* **1998**, *120*, 11 467 – 11 468; b) S. Shanmugam, A. Gedanken, *J. Phys. Chem. B* **2006**, *110*, 24 486 – 24 491; c) D. I. Foustoukos, W. E. Seyfried, Jr., *Science* **2004**, *304*, 1002 – 1005; d) N. Gokon, Y. Oku, H. Kaneko, Y. Tamaura, *Sol. Energy* **2002**, *72*, 243 – 250; e) D. U. Singh, P. R. Singh, S. D. Samant, *Synth. Commun.* **2006**, *36*, 1265 – 1271; f) S. T. Wong, J. F. Lee, S. Cheng, C. Y. Mou, *Appl. Catal. A* **2000**, *198*, 115 – 126; g) H. Näfe, S. Gollhofer, F. Aldinger, *J. Electrochem. Soc.* **2002**, *149*, E311 – 316.

[3] a) R. H. Kodama, S. A. Makhlouf, A. E. Berkowitz, *Phys. Rev. Lett.* **1997**, *79*, 1393 – 1396; b) R. H. Kodama, *J. Magn. Magn. Mater.* **1999**, *200*, 359 – 372; c) R. H. Kodama, A. E. Berkowitz, *Phys. Rev. B* **1999**, *59*, 6321 – 6336; d) I. V. Golosovsky, I. Mirebeau, G. Andre, D. A. Kurdyukov, Y. A. Kumzerov, S. B. Vakhrushev, *Phys. Rev. Lett.* **2001**, *86*, 5783 – 5786; e) J. Milano, L. B. Steren, M. Grimsditch, *Phys. Rev. Lett.* **2004**, *93*, 077601; f) W. S. Seo, H. H. Jo, K. Lee, B. Kim, S. J. Oh, J. T. Park, *Angew. Chem.* **2004**, *116*, 1135 – 1137; *Angew. Chem. Int. Ed.* **2004**, *43*, 1115 – 1117 (Corrigendum: W. S. Seo, H. H. Jo, K. Lee, B. Kim, S. J. Oh, J. T. Park, *Angew. Chem.* **2004**, *116*, 3834; *Angew. Chem. Int. Ed.* **2004**, *43*, 3749); g) L. Li, L. J. Chen, R. M. Qihe, G. S. Li, *Appl. Phys. Lett.* **2006**, *89*, 134 102 – 134 104.

[4] R. M. Cornell, U. Schwertmann, *The Iron Oxides: Structure, Properties, Reactions, Occurrence and Uses*, VCH, New York, **1996**.

[5] a) M. Yin, S. O'Brien, *J. Am. Chem. Soc.* **2003**, *125*, 10 180 – 10 181; b) S. Sun, H. Zeng, D. B. Robinson, S. Raoux, P. M. Rice, S. X. Wang, G. Li, *J. Am. Chem. Soc.* **2004**, *126*, 273 – 279; c) F. Z. Redl, C. T. Black, G. C. Papaefthymiou, R. L. Sandstrom, M. Yin, H. Zeng, C. B. Murray, S. P. O'Brien, *J. Am. Chem. Soc.* **2004**, *126*, 14 583 – 14 599.

[6] a) J. Rockenberger, E. C. Scher, A. P. Alivisatos, *J. Am. Chem. Soc.* **1999**, *121*, 11 595 – 11 596; b) T. Hyeon, S. S. Lee, J. Park, Y. Chung, H. B. Na, *J. Am. Chem. Soc.* **2001**, *123*, 12 798 – 12 801; c) S. Sun, H. Zeng, *J. Am. Chem. Soc.* **2002**, *124*, 8204 – 8205; d) W. W. Yu, J. C. Falkner, C. T. Yavuz, V. L. Colvin, *Chem. Commun.* **2004**, 2306 – 2307.

[7] R. Si, Y.-W. Zhang, L.-P. You, C.-H. Yan, *Angew. Chem.* **2005**, *117*, 3320 – 3324; *Angew. Chem. Int. Ed.* **2005**, *44*, 3256 – 3260.

